MATEMÁTICA
ESPOL - FCNM JOURNAL
2020, Vol. 18, No. 1 Enero - Junio

Modified S^2 imaging modal decomposition technique in Few Mode Fibers

Técnica de descomposición modal de imágenes modificada S^2 en fibras de pocos modos

Erick A. Lamilla Rubio

Recepción: 04/04/2020 **Aceptación:** 26/05/2020 **Publicación:** 30/06/2020

Abstract Precise knowledge of modal content in fibers that support different optical modes is important to understanding fiber properties and system performance. Several techniques have been implemented for modal content characterization in few mode fibers with the intention of identifying modes supported by these fibers. Direct modal characterization techniques have become popular for allowing a fairly accurate mode analysis as well as experimentally recover the mode amplitude and phase spatial profile. However, in some specific scenarios, certain limitations such as complete mode-recovery and resolution have to be overcome with these methods. In this paper are presented some modifications to a direct method of modal recovery that allow to remove several of those limitations. A mathematical implementation that consists of adding an external reference to the method is presented and studied, as well as the explanation of the proposed mode-recovery algorithm in detail.
Keywords optical fibers, optical modes, S^2 characterization.

Resumen El conocimiento preciso de contenido modal en fibras que soportan diferentes modos ópticos es importante para entender las propiedades de las fibras y el rendimiento de un sistema. Técnicas directas de caracterización modal se han vuelto populares por permitir un analisis de modo bastante preciso así como la recuperación experimental de la amplitud del modo y su perfil espacial de fase. Sin embargo, en algunos escenarios específicos, ciertas limitaciones tales como una recuperación completa de modos y la resolución de los mismos han tenido que superarse con estos métodos. En este trabajo son presentados algunas modificaciones a un método directo de recuperación modal que permita eliminar la mayoría de estas limitaciones. Se presenta y se estudia una implementación matemática que consiste en la adición de una referencia externa al método, así como

Erick Abraham Lamilla Rubio, Doctor of Science
Researcher/Assistant-Professor, ESPOL Polytechnic University, Escuela Superior Politécnica del Litoral, ESPOL, Facultad de Ciencias Naturales y Matemáticas (FCNM), Campus Gustavo Galindo Km. 30.5 Vía Perimetral P.O. Box 09-01-5863, Guayaquil, Ecuador, e-mail: ealamill@espol.edu.ec, https://orcid.org/0000-0002-1644-9465

la explicación detallada del algoritmo de recuperación modal propuesto.
Palabras Claves caracterización S^2, fibras ópticas, modos ópticos.

1 Introduction

The development of new fiber technology supporting different modes such as few-mode fibers has allowed a wide range of applications involving mode-division multiplexing Jung et al. (2013), particle manipulation (Schmidt, Garbos, Euser, & Russell, 2012) and non-linear optics study (Song & Kim, 2013) to name a few examples. These applications need to take into account the properties of the modes excited in the fiber, consequently, the need to characterize modes in this type of fibers stimulated the development of new methods. In this way, many techniques have been implemented for the characterization of multi-mode optical wave-guides. In the literature, these methods can be classified in two groups: modal decomposition techniques that require prior knowledge of modal profiles (Shapira, Abouraddy, Joannopoulos, & Fink, 2005) and modal characterization methods that require no a priori knowledge (Nguyen et al., 2012; J. W. Nicholson, Yablon, Ramachandran, & Ghalmi, 2008; Schimpf, Barankov, & Ramachandran, 2011). Among these two groups, the second one has become popular for its ability to directly recover modal information (amplitude and phase) and for the simplicity it presents in the experimental implementation in most cases. The Spatial and Spectral (S^2) imaging method implemented by J. W. Nicholson et al. (2008) is the most common modal characterization method used in few mode fibers (FMFs), which is capable of simultaneously imaging multiple, higher-order modes (HOMs).

S^2 imaging consists of identifying modes propagating in optical fibers by the spectral interference pattern between HOMs and the fundamental mode caused by their relative group delay difference and by the distinct spatial interference pattern (J. Nicholson et al., 2012). To explain the principle of operation of the S^2 modal decomposition technique, Fig. 1 will be used. Fig. 1(a) shows a simple experimental setup of the S^2 imaging method. The system shows a tunable laser source (TLS) where the laser light frequency is swept. The TLS is connected to a single-mode fiber (SMF) where light is coupled to a single mode of propagation, which is the fundamental mode. A positioning stage is used to align the SMF with the fiber under test (FUT). The positioning stage also allows to manipulate the launch condition including an offset and therefore, control the excitation of different modes (Lamilla, Aldaya, Serpa, Jarshel, & Dainese, 2016). The image of the beam at the output of the FUT is then magnified to be projected afterwards on the image plane and recorded by a CCD camera. Fig. 1(b) illustrates the flow chart with principle operation of the mentioned S^2 imaging method. Initially, the stack of images captured by the camera during the frequency sweep of the TLS is recorded as shown in Fig. 1(b.i). Then, all the images captured by the camera are organized in a tensor that each value correspond to a pixel (x,y) of an image captured at each frequency ω_n as shown in Fig. 1(b.ii). The images organized as a tensor according to the fre-

quency ω allow to obtain the interference pattern as shown in Fig. 1(b.ii) between the HOMs and the fundamental mode that acts as reference. The Inverse Fourier Transform (IFT) of the spectral optical intensity is then computed at a given pixel coordinate (Pixel (k,l) in Fig. 1(b.ii)) along the frequency dimension ω obtaining a new spectral optical intensity in the temporal domain τ as shown in Fig. 1(b.iv). The processed IFT contains the information of the spatial distribution of the propagating HOMs and the differential delay between these HOMs and the fundamental mode, consequently, the IFT is used to recover modes (amplitude, phase and relative power levels) as shown in Fig. 1(b.v).

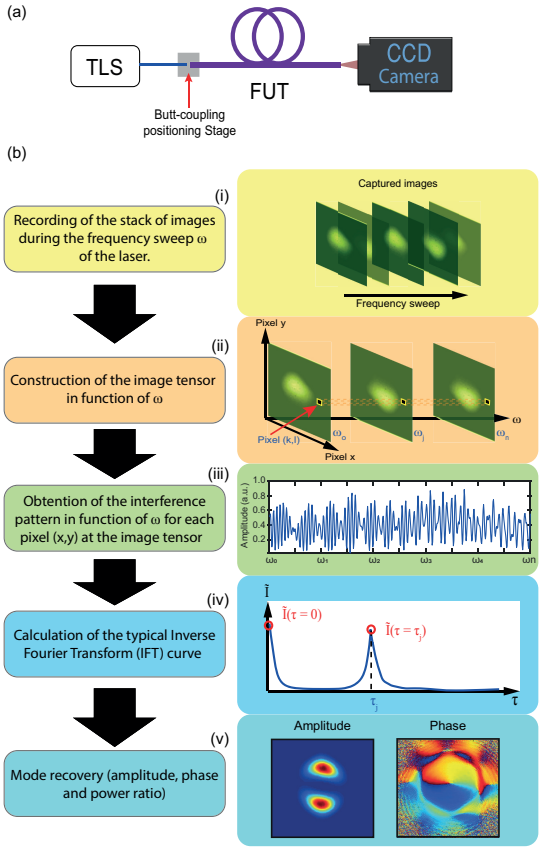

Fig. 1 (a) Basic Schematic of the typical experimental setup used for S^2 imaging method. TLS: tunable laser source; FUT: fiber under test (b) Flow chart of the principle of operation of the S^2 imaging method
Source: Own Creation

Note that, for S^2 imaging to work properly, the State of Polarization (SoP) of the fundamental mode must be aligned with the SoP of the HOMs. "If there is any difference between SoP of the fundamental mode and the HOMs, it will necessary to perform two measurements, one for each SoP" (Lamilla, 2019, p. 38) A limitation of the S^2 imaging can be seen in the fact that the technique has no control in the spa-

tial overlap between the reference fundamental mode and the higher-order modes. Consequently, modes having little intensity overlap with the fundamental mode are neglected. Another scenario where the S^2 method does not result reliable is when the fundamental mode is not dominant. This is indeed what happens in micro-structured fibers which present an attenuation region in the middle of the transmission spectrum where fundamental mode is strongly attenuated (West, Smith, Borrelli, Allan, & Koch, 2004; Amezcua-Correa et al., 2008). Another difficulty in the S^2 method can be appreciated when modes with low and high differential delay are simultaneously present in the fiber. In this case, the method have insufficient resolution to solve highly-dispersive modes (J. Nicholson et al., 2012).

To overcome the mentioned limitations, this paper proposes two modification to the S^2 imaging method: the addition of an external reference and variable sliding window IFT. The paper is organized as follows: in Section 2, the mathematical detail of these modifications are presented. In Section 3, advantages and disadvantages of the modification to the S^2 method are discussed and Section 4 concludes the paper.

2 Mathematical description of the modified S^2 method

In order to overcome the limitation of mode-recovery in the standard S^2 imaging method, two modifications to the method are implemented. The first modification is implemented in the currently experimental setup shown in Fig. 1(a), using a fraction of the incoming laser power as an external reference in a Mach-Zhender interferometer (MZI)[1] configuration, as can be observed in Fig. 2. In this configuration, light of a TLS is collimated by an objective lens L_1 and then divided using a polarization beam splitter (PBS). A polarization controller (PC) at the input of the MZI is used to control the power ratio between the reference and probe arm. The lens L_2 and L_3 are used to focus the probe arm on the fiber under test (FUT) and collimate the fiber output beam respectively. A beam splitter (BS) combines the fiber output beam with the reference beam coming from the other MZI arm. The combined beam is captured by the CCD camera, and the information of the interference pattern between the reference beam and the fiber modes is recorded.

The mathematical details of how the modified S^2 method works to recover fiber-modes are described below:

First, consider the electric field coming to the camera given by the superposition of the output fiber field and the reference field[2]:

[1] In Physics, a Mach-Zhender interferometer is an optical device used to determine the relative phase shift variations between two collimated beams derived by splitting light from a single source. The path length can be adjusted so that for a particular optical frequency, the total power goes into one of the arms.

[2] The electric field is a term used in Physics to refer to the optical field, shown as **E** in the electromagnetic wave equation which can be derived from Maxwell's Equations.

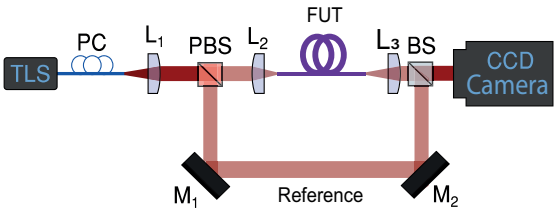

Fig. 2 Basic scheme of the experimental setup for modified S^2 imaging method. TLS: tunable laser source; PC: polarization controller; $L_{1,2,3}$: objective lens; PBS: polarization beam splitter; $M_{1,2}$: mirror; FUT: fiber under test and BS: beam splitter.
Source: (Lamilla et al., 2018)

$$\mathbf{E}_{out}(x,y,\omega) = \sum_{j=1}^{m} \mathbf{E}_j(x,y,\omega)e^{i\phi_j} + \mathbf{E}_r(x,y,\omega)e^{i\phi_r} \tag{1}$$

where the first term of Eq. 1 describes the superposition of the fiber modes and the second term described the reference field. The terms ϕ_j and ϕ_r represent the spatial phase of each field and are directly related with the optical path in the MZI.

Now, a relation is established between the amplitude of each mode $E_j(x,y,\omega)$ and the amplitude of the reference field $E_r(x,y,\omega)$:

$$E_j(x,y,\omega) = \kappa_j(x,y)E_r(x,y,\omega)e^{i\omega\tau_j} + c.c. \tag{2}$$

where $\kappa_j(x,y)$ is a constant assumed to be independent of wavelength, and τ_j is the beating period between the $j-th$ mode and the reference field. The differential delay can be written as $\tau_j = 1/c|n_jL - \Delta L|$, where n_j is the group delay index of each $j-th$ mode; L is the length of the fiber and ΔL represents the difference between the optical path in the reference and probe arm (excluding the FUT length).

It is well known that the optical intensity captured camera is proportional to the square module of the electric field (Agrawal, 1989), therefore an expression for $|\mathbf{E}_{out}(x,y,\omega)|^2$ can be calculated :

$$\begin{aligned} |\mathbf{E}_{out}(x,y,\omega)|^2 &= |\sum_{j=1}^{n} \kappa_j E_r(x,y,\omega)e^{i\phi_j} + E_r(x,y,\omega)e^{i\phi_r}|^2 \\ &= |E_r(x,y,\omega)|^2\Big(1 + \sum_{j=1}^{n}|\kappa_j|^2 + \sum_{j=1}^{n} 2\,\mathbb{R}\mathrm{e}\{\kappa_j e^{i(\phi_j-\phi_r)}\} \\ &+ \sum_{j\neq l}^{n} \kappa_j\kappa_l^* e^{i(\phi_j-\phi_l)}\Big) \end{aligned} \tag{3}$$

In Eq. 3, the term $|E_r(x,y,\omega)|^2\Big(1 + \sum_{j=1}^{n}|\kappa_j|^2\Big)$ represents the sum of the intensities of all the fiber modes including the reference beam profile, the term $|E_r(x,y,\omega)|^2\Big(\sum_{j=1}^{n} 2\,\mathbb{R}\mathrm{e}\{\kappa_j e^{i(\phi_j-\phi_r)}\}\Big)$ indicates the sum of interference pattern between each $j-th$ mode fiber with the reference beam and the last term represents the sum of interference pattern between fiber modes. The result of Eq. 3 is useful to calculate the optical intensity profile:

$$
\begin{aligned}
I_{out}(x,y,\omega) = I_r(x,y,\omega)\Bigg[1 &+ \sum_{j=1}^{n}\left|\kappa_j(x,y)\right|^2 \\
&+ \sum_{j=1}^{n} 2\left|\kappa_j(x,y)\right|\cos\left(\omega\tau_j + \varphi_{jr}\right) \\
&+ \sum_{j\neq l}^{n} 2\left|\kappa_j(x,y)\right|\left|\kappa_l(x,y)\right|\cos\left(\omega\tau_{jl} + \varphi_{jl}\right)\Bigg]
\end{aligned}
\tag{4}
$$

where $I_r(x,y,\omega)$ is the optical intensity distribution of the external reference, considered a Gaussian profile[3]. The parameter $\varphi_{jr,jl}$ in the argument of the interference patterns represents the relative spatial phase between $j-th$ fiber-modes and the external reference (jr), and between fiber-modes (jl).

Now, the inverse Fourier transform of the optical intensity shown in Eq. 4 is calculated (Lamilla, 2019):

$$
\begin{aligned}
\widetilde{I}_{out}(x,y,\tau) &= F^{-1}\left\{I_{out}(x,y,\omega)\right\} \\
&= \int_{-\infty}^{+\infty} I_{out}(x,y,\omega)e^{i\omega\tau}d\omega \\
&= \int_{-\infty}^{+\infty} I_r(x,y,\omega)\Bigg[1 + \sum_{j=1}^{n}\left|\kappa_j(x,y)\right|^2 \\
&+ \sum_{j=1}^{n} 2\left|\kappa_j(x,y)\right| cos(\omega\tau_{jr} + \varphi_{jr}) \\
&+ \sum_{j\neq l}^{n} 2\left|\kappa_j(x,y)\right|\left|\kappa_l(x,y)\right| cos(\omega\tau_{jl} + \varphi_{jl})\Bigg]e^{i\omega\tau}d\omega \\
&= \widetilde{I}_r(x,y,\tau)\Big\{\Big(1 + \sum_{j=1}^{n}|\kappa_j(x,y)|^2\Big)2\pi\delta(\tau) \\
&+ \sum_{j=1}^{n}|\kappa_j(x,y)|\Big[e^{i(\varphi_{jr})}2\pi\delta(\tau+\tau_{jr}) + e^{-i(\phi_{jr})}2\pi\delta(\tau-\tau_{jr})\Big] \\
&+ \sum_{j\neq l}^{n}|\kappa_j(x,y)||\kappa_l(x,y)|\Big[e^{i(\phi_{jl})}2\pi\delta(\tau+\tau_{jl}) \\
&+ e^{-i(\phi_{jl})}2\pi\delta(\tau-\tau_{jl})\Big]\Big\}
\end{aligned}
\tag{5}
$$

where $\widetilde{I}_{out}(x,y,\tau) = F^{-1}\left\{I_{out}(x,y,\omega)\right\}$ now is the IFT of the optical spectrum of the combined beam (reference beam and output fiber beam). Then, the value of

[3] In Optics, particularly in Laser Physics, laser beam often occur in the form of Gaussian distribution, generally with an added parabolic phase profile.

$\kappa_j(x,y)$ is calculated replacing $\tau = \tau_m$ in Eq. 5: $\widetilde{I}_{out}(x,y,\tau=\tau_m) = \widetilde{I}_r(x,y,\tau=\tau_m)|\kappa_m|e^{-i\varphi_{mr}}2\pi\delta(0)$.

Then, the value of $\kappa_m(x,y)$ is:

$$\kappa_m(x,y) = \Big[\frac{\widetilde{I}_{out}(x,y,\tau=\tau_m)}{2\pi\widetilde{I}_r(x,y,\tau=\tau_m)}\Big]^* \tag{6}$$

Finally, the value of $\kappa_m(x,y)$ can be used in Eq. 2 to recover the mode-field profile (amplitude and relative spatial phase).

The second modification to the S^2 method consists on varying the frequency window in the IFT, which is implemented in the S^2 data. Tipycally, S^2 measurements in the format of spectrogram with sliding window Fourier transform of the beating signal can be used to observe slight modifications of the differential delay between modes over the measured frequency region (Jasapara & Yablon, 2012; Newkirk et al., 2016; Carpenter, Eggleton, & Schröder, 2016). However, the use of a uniform sliding window would allow identifying and solving either low-dispersive or highly-dispersive modes, depending on the frequency resolution chosen; but it will not be possible to solve both types of modes simultaneously. For this reason, the implementation of a non-uniform sliding window in the IFT is required to properly recover both types of modes.

The pseudo-code shown in the flow-chart in Figure 3 is used to explain the implementation of a non-uniform sliding window in the IFT. Consider the variables M, ω_{array}, $\omega_{t-array}$ and N_ω obtained from the images capture and experimental measurements using the setup of Fig. 2. M represents the $I_{out}(x,y,\omega)/I_r(x,y,\omega)$ tensor obtained in the modified S^2 analysis; ω_{array} is the frequency array obtained in the laser frequency sweep; $\omega_{t-array}$ is the range of frequency where the transition of the window size will be applied in the IFT and N_ω accounts as the length of ω_{array}.

To calculate the spectrogram using the localized IFT, the following variables should be initialized (See initialization variables in the flow-chart of Fig. 3): `OF` that represents the overlap factor is set to 0.8 (that is contiguous frequency windows are overlapped by 80% for this example); S_{out} that represents the counter for the current initial sample is set to 1. The variable $\omega_{adap-ref}$ represents the frequency array of the reference signal and takes the value of ω_{array}; while $\omega_{adap-win}$ represents a raised cosine interpolation between ω_{array} and $\omega_{t-array}$. The variable ω_{win} takes the values of the linear interpolation between $\omega_{adap-ref}$ and $\omega_{adap-win}$; ω_c accounts as the initial central frequency, and N_{win} is the size of the first window.

A *Loop While* is used during the calculation process of the spectrogram matrix `Spec-Mtx`, which is carried out while the condition $S_{aux} + N_{win} < N_\omega$ is true. First, ω_{win} and N_{win} are re-calculated using the Nyquist criterion (see flow-chart Fig. 3). Then, the tensor M_{win} is created in order to store the elements of M according to the iteration order; from the element S_{aux} to the element $S_{aux} + N_{win} - 1$. Consequently, the IFT of M_{win} is calculated and stored in the tensor m_{win}. Finally, the central frequency ω_c and the subsequent element S_{aux} are re-calculated using the new values of ω_{win}, N_{win} and the overlap factor `OF` (overlap factor calculation box in Fig. 3).

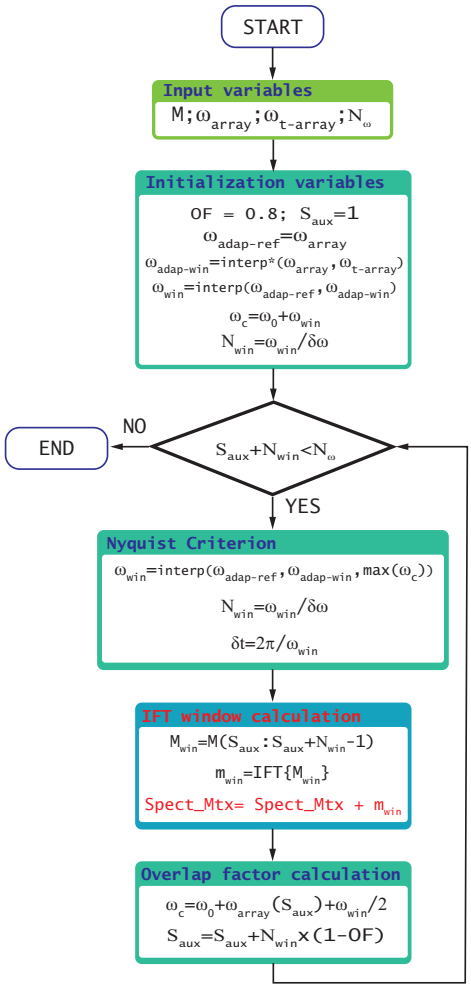

Fig. 3 Pseudo-code of the algorithm to calculate a variable sliding window Inverse Fourier Transform. The input/output variables, the Nyquist criterion and IFT window calculation are identified in each process.
Source: Own creation

3 Discussion

The modifications implemented to the S^2 imaging method allowed to overcome the limitations to recover highly-dispersive modes and modes with high-slope differential delay. It is important to note that, since the reference beam does not traverse the fiber under test, it is not affected by the high attenuation region in the middle of the transmission spectrum, thus keeping its power constant over a broad frequency range. Another advantage is that the spot size of the reference can be controlled to completely overlap with all modes propagating in the fiber. The implementation of a variable sliding window IFT in the S^2 method also allows to avoid the trade-off between the resolution in frequency and time domain. Depending on the

frequency window in the spectrogram, it is possible to distinguish between traces with relative flat differential delay curves, and high-slope curves corresponding to highly-dispersive modes. The modified S^2 method proposed in this work has been tested and has been used successfully to characterize surface modes in a hollow-core photonic-crystal fiber (Lamilla et al., 2018), which have a highly-dispersive nature.

4 Conclusion

In this paper, the mathematical description of a modification of the S^2 imaging technique is explained in details. The modified S^2 imaging technique, applied to interferometric data, allow to recover low and highly-dispersive modes. Applying this modified S^2 technique in a variable window Inverse Fourier Transform, it is possible to recover highly-dispersive surface-modes in a hollow-core photonic-crystal fiber, as a particular example.

5 Acknowledgements

I thank FAPESP (grants 2013/20180-3, 2015/04113-0, 08/57857-2, 2013/20180-3, 08/57857-2) CAPES and CNPq (grant 574017/2008-9). A special thanks to my PhD advisor Prof. Dr. Paulo Dainese and my laboratory colleagues Dr. Ivan Aldaya, Dr. Paulo Jarschel, Dr. Julian Pita, MSc. Omar Florez and Eng. Letícia Magalhães that helped me with their ideas and their company during my PhD program.

6 Bibliography

References

Agrawal, G. P. (1989). Nonlinear fiber optics, chap. 5. *AT&T–Academic press Inc*.

Amezcua-Correa, R., Gérôme, F., Leon-Saval, S. G., Broderick, N. G. R., Birks, T. A., & Knight, J. C. (2008). Control of surface modes in low loss hollow-core photonic bandgap fibers. *Opt. Express*, *16*(2), 1142–1149. doi: 10.1364/OE.16.001142

Carpenter, J., Eggleton, B. J., & Schröder, J. (2016). Polarization-resolved cross-correlated (c2) imaging of a photonic bandgap fiber. *Opt. Express*, *24*(24), 27785–27790. doi: 10.1364/OE.24.027785

Jasapara, J., & Yablon, A. D. (2012). Spectrogram approach to s2 fiber mode analysis to distinguish between dispersion and distributed scattering. *Opt. Lett.*, *37*(18), 3906–3908. doi: 10.1364/OL.37.003906

Jung, Y., Sleiffer, V. A. J. M., Baddela, N., Petrovich, M. N., Hayes, J. R., Wheeler, N. V., ... Richardson, D. J. (2013). First demonstration of a broadband 37-cell hollow core photonic bandgap fiber and its application to high capacity mode division multiplexing. In *2013 optical fiber communication conference and exposition and the national fiber optic engineers conference (ofc/nfoec)* (p. 1-3).

Lamilla, E. (2019). Characterization and manipulation of optical modes in photonic crystal fibers: Caracterização e manipulação de modos ópticos em fibras de cristal fotônico. *Repositorio.Unicamp.br*. Retrieved from `http://repositorio.unicamp.br/jspui/handle/REPOSIP/335703`

Lamilla, E., Aldaya, I., Serpa, C. M., Jarshel, P., & Dainese, P. C. (2016). Modal content in a 7-cell hollow-core photonic bandgap fiber and its dependence with offset launch conditions. In *Latin america optics and photonics conference* (p. LTu3C.3). Optical Society of America. doi: 10.1364/LAOP.2016.LTu3C.3

Lamilla, E., Faria, M. S., Aldaya, I., Jarschel, P. F., Pita, J. L., & Dainese, P. (2018). Characterization of surface-states in a hollow core photonic crystal fiber. *Opt. Express*, *26*(25), 32554–32564. doi: 10.1364/OE.26.032554

Newkirk, A. V., Antonio-Lopez, J. E., Anderson, J., Alvarez-Aguirre, R., Eznaveh, Z. S., Lopez-Galmiche, G., ... Schülzgen, A. (2016). Modal analysis of antiresonant hollow core fibers using s2 imaging. *Opt. Lett.*, *41*(14), 3277–3280. doi: 10.1364/OL.41.003277

Nguyen, D. M., Blin, S., Nguyen, T. N., Le, S. D., Provino, L., Thual, M., & Chartier, T. (2012). Modal decomposition technique for multimode fibers. *Appl. Opt.*, *51*(4), 450–456. doi: 10.1364/AO.51.000450

Nicholson, J., Meng, L., Fini, J., Windeler, R., DeSantolo, A., Monberg, E., ... Ortiz, R. (2012). Measuring higher-order modes in a low-loss, hollow-core, photonic-bandgap fiber. *Opt. Express*, *20*(18), 20494–20505. doi: 10.1364/OE.20.020494

Nicholson, J. W., Yablon, A. D., Ramachandran, S., & Ghalmi, S. (2008). Spatially and spectrally resolved imaging of modal content in large-mode-area fibers. *Opt. Express*, *16*(10), 7233–7243. doi: 10.1364/OE.16.007233

Schimpf, D. N., Barankov, R. A., & Ramachandran, S. (2011). Cross-correlated (c2)

imaging of fiber and waveguide modes. *Opt. Express*, *19*(14), 13008–13019. doi: 10.1364/OE.19.013008

Schmidt, O. A., Garbos, M. K., Euser, T. G., & Russell, P. S. J. (2012). Metrology of laser-guided particles in air-filled hollow-core photonic crystal fiber. *Opt. Lett.*, *37*(1), 91–93. doi: 10.1364/OL.37.000091

Shapira, O., Abouraddy, A. F., Joannopoulos, J. D., & Fink, Y. (2005). Complete modal decomposition for optical waveguides. *Phys. Rev. Lett.*, *94*, 143902. doi: 10.1103/PhysRevLett.94.143902

Song, K. Y., & Kim, Y. H. (2013). Characterization of stimulated brillouin scattering in a few-mode fiber. *Opt. Lett.*, *38*(22), 4841–4844. doi: 10.1364/OL.38.004841

West, J. A., Smith, C. M., Borrelli, N. F., Allan, D. C., & Koch, K. W. (2004). Surface modes in air-core photonic band-gap fibers. *Opt. Express*, *12*(8), 1485–1496. doi: 10.1364/OPEX.12.001485